HHS Public Access

Author manuscript

Nat Commun. Author manuscript; available in PMC 2015 May 05.

Published in final edited form as:

Nat Commun. ; 5: 5126. doi:10.1038/ncomms6126.

Regulation of the $Na_v1.5$ cytoplasmic domain by Calmodulin

Sandra B. Gabelli[1,2,3,*], **Agedi Boto**[1], **Victoria HalperinKuhns**[2], **Mario A. Bianchet**[1,4], **Federica Farinelli**[2], **Srinivas Aripirala**[1], **Jesse Yoder**[1], **Jean Jakoncic**[5], **Gordon F. Tomaselli**[2,*], and **L. Mario Amzel**[1,*]

[1]Structural Enzymology and Thermodynamics Group. Department of Biophysics and Biophysical Chemistry, Johns Hopkins University School of Medicine, 725 N Wolfe St, WBSB 608, Baltimore, Maryland 21205, USA

[2]Division of Cardiology, Department of Medicine, Johns Hopkins University School of Medicine, 720 Rutland Avenue, Ross Bldg. 844, Baltimore, MD 21205, USA

[3]Department of Oncology, Johns Hopkins University School of Medicine, Baltimore, MD 21287, USA

[4]Department of Neurology, Johns Hopkins University School of Medicine, 600 N Wolfe St, Baltimore, MD 21287, USA

[5]Brookhaven National Laboratory, National Synchrotron Light Source, Upton, NY 11973

Abstract

Voltage gated sodium channels (Na_v) underlie the rapid upstroke of action potentials (AP) in excitable tissues. Binding of channel interactive proteins is essential for controlling fast and long term inactivation. In the structure of the complex of the carboxy-terminal portion of $Na_v1.5$ ($CTNa_v1.5$) with Calmodulin (CaM)–Mg^{2+} reported here both CaM lobes interact with the $CTNa_v1.5$. Based on the differences between this structure and that of an inactivated complex, we propose that the structure reported here represents a non-inactivated state of the $CTNa_v$, i.e., the state that is poised for activation. Electrophysiological characterization of mutants further supports the importance of the interactions identified in the structure. Isothermal titration calorimetry experiments show that CaM binds to $CTNa_v1.5$ with high affinity. The results of this study provide unique insights into the physiological activation and the pathophysiology of Na_v channels.

Introduction

Voltage gated sodium channels (Na_v) are transmembrane glycoproteins that underlie the rapid upstroke of action potentials (AP) in excitable tissues such as the heart, skeletal muscle

*To whom correspondence should be addressed: mamzel@jhmi.edu (L.M.A); gabelli@jhmi.edu (S.B.G.); gtomasel@jhmi.edu (G.T.).

Contributions

SBG, AB, VHK, MAB, FF, SA, JY and JJ performed experiments. SBG, MAB, FF analyzed data. SBG, GFT and LMA designed and supervised research. SBG, MAB, GFT and LMA wrote the manuscript.

Competing financial interests: The authors declare no competing financial interests.

Accession codes: Coordinates and structure factors have been deposited in the Protein Data Bank with accession code 4OVN.

and brain. Mendelian inherited mutations in Na_v channels result in diseases of excitability such as myotonias, paralyses, cardiac arrhythmias, and ataxias and seizure disorders [1]. Na channels consist of an α subunit and one or more β subunits, but only the pore-forming α subunit is essential for function. Ten different isoforms of mammalian α subunits ($Na_v1.1$–1.9, and Na_x) have been described, with different properties and tissue distribution.

The transmembrane portion of the α subunit is formed by four homologous domains (DI-DIV), each containing six membrane-spanning helices (S1-S6) that form the ion selective pore and contain the activation voltage sensors. Channel activation and opening is followed by prompt closure via a number of kinetically distinct inactivation states[2]. Fast inactivation (recovery τ <10 msec), the best characterized of these processes, involves occlusion of the cytoplasmic mouth of the channel by the interdomain DIII-DIV linker (DIII/IV). A triplet of hydrophobic residues of the linker, Ile-Phe-Met (IFM), is key for this inactivation [3].

Na_V channels are regulated by the interaction of their carboxyl terminal (CT) domain, located in the cytoplasm of responsive cells, with various channel interactive proteins (CIP) [4,5]. The importance of these interactions is highlighted by the effects of mutations in the Na_v CT domain ($CTNa_v$) on channel function: gain-of-function mutations of the $Na_V1.5$ CT domain (CT $Na_v1.5$) cause long QT syndrome and loss-of-function mutations result in Brugada syndrome.

The proximal portion of the $CTNa_v$ (residues 1776–1929 in $Na_v1.5$) is comprised of six α-helices (αI-αVI) [6,7]. The first four helices αI-αIV, form an EF-hand like motif (EFL) that has a fold similar to that of a Ca^{2+}-binding EF hand [8–10]. The fifth helix (αV) and a flexible loop connect the EFL to a long sixth helix (αVI) which contains an IQ motif that binds calmodulin (CaM)[7].

Several structural studies have explored the interaction of CaM with different regions of Na_v channels. One structure, the complex of the C-lobe of CaM with the DIII/IV linker of Na_V channels, suggests that CaM modulates fast inactivation by forming a bridge between the $CTNa_v$ IQ motif and the DIII/IV linker of the channel [11,12]. In the structure of the ternary complex containing $CTNa_V1.5$, apo-CaM and a fibroblast growth factor homologous factor (FHF)—a long-term inactivator of Na_v channels—FHF binds to the EFL of $Na_v1.5$ and the C-lobe of CaM binds to the IQ motif[7]. Together, these structural data point to complex dynamic interactions among the participating components in regulating channel gating.

Despite the availability of biochemical, electrophysiological, biophysical and structural information, the participation of the $CTNa_v$ in the regulation of Na_V channels is still a matter of debate and may be isoform-specific [8,13,14]. Given the central importance of Na_V1 channels, it is surprising that important details of the molecular mechanisms leading to their activation, inactivation and recovery from inactivation remain unknown. Missing, for example, are structures involving the cytoplasmic domain of $Na_v1.5$ when the channel is poised for opening.

Here we present the structure of the complex of the C-terminal domain of the $Na_v1.5$ channel with CaM-Mg^{2+}, which we propose, represents the resting state of the cytoplasmic region of the channel after the recovery from inactivation; i.e. the state in which the channel

is poised for activation. We will refer to this state as "non-inactivated" or resting. Site-specific mutations at the sites of interactions identified in the structure presented here alter the inactivation properties of $Na_v1.5$ as determined by electrophysiological recordings. Calorimetric measurements show that $CTNa_v1.5$ binds tightly to full length CaM, while the DIII-IV linker peptide cannot compete CTNav1.5 from the $CTNa_v1.5$-CaM complex. The results of this study provide unique insights into the physiological activation and the pathophysiology of Na_v channels.[15]

Results

Overall structure of the $CTNa_v1.5$-CaM complex

The crystal of the $CTNa_v1.5$-CaM-Mg^{2+} complex (see below) determined to 2.8 Å contains 5 highly similar heterodimers in the asymmetric unit (average rms deviation 1.6 Å), each composed of a full length calmodulin (residues 1–148) and one $CTNa_v1.5$ (residues 1776–1929) (Table 1, Fig. 1, Supplementary Table 1).

In each heterodimer the $CTNa_v1.5$ has a bipartite structure resembling a lollipop (Fig. 1a) in which the globular EFL domain (residues 1776 –1866), the head, is connected via helix αV (residues 1866 to 1884) and a loop (residues 1885 to 1894) to the long stalk (helix αVI; residues 1895–1929) (Fig. 1a). The structure of the EFL domain (helices αI-αIV; Fig. 1) is similar to the NMR structures of the EFL domains of $Na_v1.5$ (residues 1773–1865, PDB id 2KBI, Supplementary Table 2) [16] and $Na_v1.2$ (pdb id 2KAV)[17].

Calmodulin conformation in the $Na_v1.5$-CaM-Mg^{2+} complex

The CaM N-lobe (residues 1 to 77; helices αA to αD; Supplementary Fig. 1) adopts a "closed" conformation and the C-lobe (residues 82–148; helices αE to αH) a "semi open" conformation (Supplementary Fig. 1, Supplementary Fig. 2)[18–20]. A short linker (residues 78–81) connects the two lobes in such a way that the long axis of helix αD of the N- lobe (residues 65–77) is orthogonal to the αE helix of the C- lobe (residues 82–93) forming a "lock-washer" type arrangement around helix αVI of the $CTNa_v1.5$ (Fig. 1a). This conformation of CaM is highly different from the one observed in the structure of the $CTNa_v1.5$-CaM-FGF13[7] complex (pdb id 4DCK; FGF: fibroblast growth factor; FGF13=FHF2) in which helix αD, the linker, and helix αE form a long nine-turn helix (residues 64–95) that places the CaM N-lobe at a significant distance from the $CTNa_v1.5$.

Ion binding in the $Na_v1.5$-CaM-Mg^{2+}complex

Both calmodulin lobes of all five CaMs in the asymmetric unit contain bound ions. The lack of anomalous scattering signal at Cu Kα, a wavelength at which Ca^{2+} and Mn^{2+} have significant anomalous signal, and the observed coordination suggest that the ions are Mg^{2+} from the crystallization solution [19] (Supplementary Fig. 1). Significantly, the conformation of the N- lobe of CaM in the $Na_v1.5$-CaM-Mg^{2+} complex reported here is highly similar to that of N-lobe of apoCaM (pdb id 1DMO [18]; Supplementary Fig. 1) as well as to the N-lobe-CaM-Mg^{2+} complex (pdb id 3UCW; Supplementary Table 3[19]) . In contrast, it is significantly different from that of the Ca^{2+}-loaded CaM (pdb id 1CDM [21]). The C-lobe of CaM in the $Na_v1.5$-CaM-Mg^{2+} complex has the semi-open conformation observed in CaM

structures such as that of $Na_v1.2$-IQ-CaM complex in which the cation binding sites are *not* occupied by Ca^{2+} (pdb id 2KXW; pdb id 3WFN, Supplementary Fig. 2)[22,23].

No ions are bound to the $CTNa_v1.5$ EFL domain in the $CTNa_v1.5$-CaM-Mg^{2+} complex. This domain does not show density at the expected ion positions ("Ca^{+2} binding loops"; residues 1802–1812 and residues 1838–1850), and crucial acidic residues such as Glu1804 and Glu1846 are not in the conformations required for Ca^{+2} binding (Supplementary Fig. 2).

$CTNa_v1.5$-CaM Interaction

In the complex reported here, CaM wraps around the long helix of $Na_v1.5$ in such a way that the interface buries approximately 1400 $Å^2$ (Supplementary Table 4), ~ 950 $Å^2$ between the C-lobe of CaM and the $CTNa_v1.5$ IQ, and ~ 450 $Å^2$ between of the N-lobe and the $Na_v1.5$ EFL domain. The CaM-$CTNa_V1.5$ interface is mostly hydrophobic (29 EFL hydrophobic interactions; Fig. 2a, b) but it is flanked at both ends by hydrogen bonds between the two proteins (7 H-bonds: Lys1899-Glu12, and Asn1831-Glu15, at one end and Arg1910-Asp81, Arg1913-Glu121, Arg1913-Glu115, Arg1919-Glu124, and Glu1901-Lys95 at the other; Fig. 2c).

Interaction of $CTNa_v1.5$ EFL domain and the $CTNa_v1.5$ helix αVI

In the crystal structure reported here, the EFL domains (1776–1882) of each $CTNa_v1.5$ molecule contacts the C-terminal portion of helix αVI (1910–1926) of another $CTNa_v1.5$ molecule, (Fig. 3). This $CTNa_v1.5$-$CTNa_v1.5$ interaction (buried area ~900 Å; complementarity index 0.55[24]) is also mainly hydrophobic. It is flanked at both ends by salt bridges (Glu1804-Arg1910, Glu1799-Arg1914, and Asp1792-Lys1922) and hydrogen bonds (Tyr1795-Arg1914, and Asn1883-Ser1920) (Fig. 3 and Fig. 4). A helix αVI-EFL interaction was postulated by Chazin and coworkers, and measured by Glaaser by transition-metal ion FRET[16,25] but it was interpreted as an intramolecular interaction and not as an interaction between two molecules.

Calorimetric Analysis

Isothermal titration calorimetry at 28 ° C (Fig. 5a) shows that $CTNa_v1.5$ binds CaM in an exothermic reaction with K_ds ranging from 46±33 to 105±15 nM depending on the buffer conditions. The lack of significant enthalpies of binding of the III-IV linker to the $CTNa_v1.5$-CaM complex argues against the competition between III-IV and the C-lobe of CaM (Fig. 5b).

Size Exclusion Chromatography of the $CTNa_v1.5$-CaM—SEC analysis shows that, in solution, CTNav1.5-CaM behaves as a heterodimer with a retention time corresponding to a complex with one molecule of $CTNa_v1.5$ and one of CaM (Supplementary Fig. 3). The elution profile shows no indication of the presence of oligomers of this heterodimer.

DISCUSSION

The most intriguing feature of the structure presented here is the presence of an intimate contact between the C-terminal portion of the $Na_v1.5$ helix αVI and the EFL domain of

another $Na_v1.5$ molecule in an arrangement that can be described as an asymmetrical [$CTNa_v1.5$-CaM]- [$CTNa_v1.5$-CaM] homodimer (Fig. 1, Fig. 3, and Fig. 4). This dimer may reflect the $Na_v1.5$-$Na_v1.5$ interaction reported in cells. Full length $Na_v1.5$ was shown by co-immunoprecipitation to form homodimers when expressed in cells [26,27]. Moreover, this dimerization of Nav1.5 explains the effect of some dominant-negative disease-causing mutations. Although there is no direct evidence that the interface observed in the structure described here is part of this dimerization, there are other strong indications that the contact described in this manuscript is part of an important physiological interaction. First, *all* five $Na_v1.5$ monomers in the asymmetric unit participate in this exact same contact. The rms deviations among the structures of the five heterodimers in the asymmetric unit range from 1.2 to 1.7 Å (for 270 Cα carbons aligned), indicating that this organization of two $Na_v1.5$ and two CaM molecules is conserved regardless of crystal contacts. Had these contacts only been present between molecules related by crystal symmetry an argument could have been made that they are a consequence of crystal packing. That all molecules in the asymmetric unit make this contact points to a fundamental interaction.

Second, this contact buries about 900 $Å^2$ with a complementarity index of 0.55 (Supplementary Table 5). These values are more compatible with a true protein-protein interaction than with a crystal contact. Confirming this assessment, PISA[28], the standard software for identifying protein-protein interactions, recognizes the interface between all complexes in the asymmetric unit, G and F, F and J, J and H, I and H, and I and G[24], as true dimers. Furthermore, residues that participate in this interface are well-conserved among Na_v isoforms (Supplementary Fig. 4).

Third, in the dimer, the N-termini of the two $CTNa_v1.5$ monomers point in the same direction. This arrangement allows the N-terminal of both $CTNa_v1.5$ to simultaneously emerge as continuations of the helices S6 of their respective channels (Fig. 5c). In addition, in this arrangement, there are no clashes of any portion of the dimer of complexes ($Na_v1.5$-CaM) with the membrane (Fig. 5c). The functional (physiological) effect of this dimerization is discussed in the next section.

The presence of a dimer of this construct is not detectable by size-exclusion chromatography (SEC) even at the highest concentrations achievable in solution (Supplementary Fig. 3). This is not surprising. While the $CTNa_v1.5$ is connected to the rest of the channel it is constrained to a very small volume close to the cytoplasmic side of the membrane (2D case) resulting in a very high local concentration. In contrast, in solution the molecules are free to occupy any position in the bulk (3D case). This effect was discussed extensively before[29–31]. The case for dimerization of the cytoplasmic portion of $Na_v1.5$ is further strengthen by the observation that the full length channel participates in functional dimers.

The physiological relevance of the structure reported here can be recognized by comparing it with that of $CTNa_v1.5$ in complex with CaM and FHF2. FHF2 has been shown to promote long term inactivation of Na_v channels [5,32,33]. This observation can be construed as suggesting that binding of the FHF stabilizes an *inactivated* conformation of the channel by locking the complex of $CTNa_v1.5$ and CaM in a configuration that is not compatible with

channel conductance. This conformation of the CTNa$_v$1.5-CaM portion of the complex shows large differences with the structure reported here.

In the CTNa$_v$1.5-CaM-FGF13 (heterotrimer), CaM is in an extended conformation in which CaM helices αD-αE are fully extended, forming a single helix that includes the linker residues. The only interaction of CaM with the CTNa$_v$1.5 involves binding of the CaM C-lobe to the IQ motif. Because of the CaM extended conformation, the CaM N-lobe lies away from the CTNa$_v$1.5 in a position that would allow it to interact with the DIII-IV linker. In contrast, in the CTNa$_v$1.5-CaM structure, CaM is present in a conformation resembling a "lock-washer" that allows its N-lobe to make significant contacts with the EFL domain of Na$_v$1.5 (area buried 450 Å^2, Fig. 6). Although the interaction of the CaM C-lobe with the IQ of helix αVI is the same in both complexes, in the structure of the complex reported here, the relation between helix αVI and the EFL domain is markedly different: helix αVI is rotated by approximately 90 ° around its axis (Fig. 5). Changes in the conformation of residues 1892 to 1895 of the Na$_v$1.5, which link the EFL-domain to helix αVI, accommodate this rotation without significant changes in either the long helix or the rest of the EFL domain. This configuration of the Na$_v$1.5-CaM heterodimer is incompatible with the mode of binding of FGF13 in the tripartite inactivated complex. Based on these key differences, we propose that the structure reported here represents the *non-inactivated* (resting) state of the cytoplasmic portion of the Na$_v$1.5, i.e., the configuration that is poised for opening of the channel. In this configuration the heterodimer can form the asymmetric CTNa$_v$1.5-CaM/CTNa$_v$1.5-CaM homodimer described above. This dimerization stabilizes the non-inactivated conformation of the channel.

In summary, the conformation of the CTNa$_v$1.5-CaM heterodimer appears to control the state of the channel. When in the conformation observed in the Na$_v$1.5-CaM-FGF13 complex the channel is inactivated—it cannot conduct. This conformation is stabilized by binding FHFs. In the structure reported here, the CaM N-lobe interacts with the Na$_v$1.5 EFL. As a result, the C-lobe changes its orientation with respect to the EFL by 90 ° and rotates with it helix αVI to the conformation that is ready for activation, i.e. the non-inactivated state. This conformation is stabilized by the formation of the CaM-Na$_v$1.5 -Na$_v$1.5-CaM homodimer.

We propose that under physiological conditions, when the two CTNa$_v$1.5 that form the homodimer are connected to the rest of their channels, only one of the two channels becomes non-inactivated and ready to open. Activation through the formation of an asymmetric homodimer has been proposed for another membrane protein, the EGF tyrosine kinase receptor, also based on an interaction observed in the crystal structure of its cytoplasmic C-terminal domain[34].

All CaM molecules in the structure reported here contain Mg^{2+} in their EF hands and therefore adopt the conformation observed in the structures of other CaM-Mg^{2+} complexes and in the structures of apo-CaM. The arrangement of the CTNa$_v$1.5 and CaM in the homodimers is not compatible with the CaM conformation of the CaM-Ca^{2+} complexes, indicating that the non-inactivated state can only be achieved with apo or Mg^{2+}-bound CaM. Since the cellular concentration of Mg^{2+} is maintained in the range 0.5–1.0 mM—i.e., above

the K_d of CaM for Mg^{2+} —CaM most likely binds Mg^{2+} during the portion of the cycle when Ca^{2+} is at its resting concentration. Thus, when the channel changes from inactivated to non-inactivated, Ca^{2+} ions bound to the CaM EF hands are replaced by Mg^{2+}, allowing the N-lobe to interact with the EFL domain and favoring formation of the $Na_v1.5$-$Na_v1.5$ homodimer.

Using the available structures, many mutations observed in cardiac arrhythmias map to the interfaces of CT$Na_v1.5$ with CIPs or other regions of the channel including the DIII-IV linker. For example, Q1909R, associated with LQT3, produces a substantial depolarizing shift in steady-state inactivation (Fig. 7 and Table 2). Another mutation Q1909A destabilizes CaM binding to the CT$Na_v1.5$ IQ domain in vitro (Table 2[13], Supplementary Fig. 5). In contrast, a mutation at the adjacent position, R1910A, has no significant effect on channel gating. (Table 2, Supplementary Fig. 5).

The physiological effects of many mutations in the CT were previously difficult to understand. Some of these can now be explained using the $Na_v1.5$-$Na_v1.5$ homodimer interface identified here (Fig. 7). For example, the mutation of K1922A produces a depolarizing shift in steady state inactivation. Interestingly, K1922 is involved in a salt bridge that links helix VI to EFL residue E1788 (Fig. 4, Fig. 7). Rotation of helix αVI in the inactivated conformation disrupts this interaction (Fig. 5d). In contrast, mutations of R1914, which is part of the same interface, produce a smaller shift in gating (Table 2, Supplementary Fig. 5). Residues 1924 and 1914, mutated in Brugada syndrome, are at the $Na_v1.5$-$Na_v1.5$ interaction interface. A1924T was predicted to be at the CaM-IQ motif interface [35]; however Chazin and coworkers showed that this residue was not in contact with CaM but with the EFL domain and suggested that the alanine residue is in a dynamic region as a possible explanation[36]. The structure of the CT$Na_v1.5$-CaM provides a direct explanation for the dysfunction: the *intermolecular* interaction of the $Na_v1.5$ helix αVI with the $Na_v1.5$-EFL- domain of another channel (Fig. 7), brings residue 1924 in close proximity to residues Met1851 and Met1875 of the interacting CT$Na_v1.5$ (Fig. 7).

Other mutations that result in significant alterations in inactivation of gating include mutations in the $Na_V1.5$-$Na_V1.5$ interface that can only be explained by the structure reported here. Notably, mutations in the αI helix of the EFL (e.g. D1790G and E1788A/D1790A/D1792A/E1799A) markedly shift the steady state inactivation ($V_{0.5}$) in the hyperpolarizing direction and result in slow recovery from inactivation (Table 2).

Direct binding measurements provided additional information about binding among cytoplasmic components. Based on ITC experiments, Sarhan *et al*. suggested that the DIII-IV linker of $Na_v1.5$ (residues 1489–1522) binds the C-lobe of CaM (K_d≈19 μM) and that this is the sole anchor point of binding of the DIII-IV peptide. In the structure reported here, however, the IQ portion of the helix αVI of $Na_v1.5$ binds to the same region of CaM as the DIII-IV linker but in the opposite orientation (Supplementary Fig. 6). In solution, CTNav1.5 binds CaM with high affinity (Kd≈50 nM). The ITC titration of the CT$Na_v1.5$-CaM complex with the DIII-IV linker peptide (see Methods) does not show significant enthalpy of binding, suggesting that the DIII-IV linker may not be able to displace the IQ from CaM binding (Fig. 5b). This result suggests that after a dimerized channel opens a change takes

place in the $Na_v1.5$-$Na_v1.5$ interaction that releases one of the two lobes of CaM for fast inactivation by DIII-IV binding (Fig. 8). We propose that as part of this change, it is the N-lobe of CaM that is released from its interaction with the EFL and binds the DIII/IV of the same channel. Additionally, we also propose that the C-lobe of CaM remains bound to the IQ and that the linker between the two CaM lobes adopts the extended helical configuration observed in the Nav1.5-CaM-FHF structure. This arrangement would set up Nav1.5 for binding FHF for long-term inactivation. A schematic representation of the relevant states is shown in Fig. 8. An important question can be asked: How does the increase in the intracellular Ca^{2+} concentration affect these states? One possible explanation is that Ca^{2+} ions will bind to CaM and change its conformation, including the conformation of both lobes. These changes would have a significant impact on the way that CaM interacts with the CTNav1.5 and as a result, on the regulation of channel activation.

The intricate set of interactions observed in the structure of the complex presented here, that includes binding of both CaM lobes to the CT $Na_v1.5$ as well as an apparent asymmetric dimerization of two $Na_v1.5$s, suggests a basis for an exquisite mechanism for switching from the inactivated to the non-inactivated form of the $Na_v1.5$ channel (Fig. 8). This model also provides a rationale for disease causing mutations that until now have escaped explanation.

Methods

Cloning

cDNA corresponding to amino acids 1773–1929 of the *H. sapiens* $Na_v1.5$ sodium channel α-subunit (CT $Na_v1.5$) was cloned into the pGEX-6-P1 vector. The entire *H. sapiens* CaM gene was cloned into the pET24b vector using the BamHI and NdeI sites.

Expression and Purification of the CT $Na_v1.5$-CaM complex

B834 (DE3) methionine auxotroph cells were transformed with both the CT $Na_v1.5$-containing and CaM-containing plasmids simultaneously. The cells were grown overnight at 37 °C in 50 mL of LB medium supplemented with 50 μg mL^{-1} kanamycin and 100 μg mL ampicillin. The overnight culture was centrifuged, the LB media was discarded, and the cells were resuspended in 50 mL of 1xM9 media containing 50 μg mL kanamycin and 100 μg mL^{-1} ampicillin. 10 mL of the resuspension was used to inoculate 1 L of M9 media containing 0.05 mg mL^{-1} selenomethionine, 50 μg mL^{-1} kanamycin, 100 μg mL^{-1} ampicillin, and additives as described by Leahy et al[37]. The cells were grown at 37 °C to an absorbance of 0.6 and protein expression was induced with 0.1 mM IPTG. The cells were grown for an additional 5 hours, centrifuged, and the pellet was frozen at −80 °C.

After thawing, pellets were resuspended in 40 mL 1x PBS with a mixture of protease inhibitors: 2 μg mL^{-1} pepstatin A, 50 μg mL^{-1} leupeptin, and 35 μg mL^{-1} PMSF per liter of culture. An additional 40 mL of 1x PBS containing 2 mg mL^{-1} lysozyme were added, along with Triton X-100 to bring the final detergent concentration to 1%. The solution was incubated at 4° C for 1.5 hours with shaking, sonicated on ice in 15 seconds bursts for a total of 1 minute, and spun at 15,000 rpm for 30 minutes. The supernatant was filtered through a

0.22 μm PES filter, and loaded on a 25 mL Glutathione Sepharose 4 Fast Flow resin using a hydrostatic pump at 0.5 mL minute^{-1}. The column was washed with 1x PBS at 1 mL minute^{-1} for a total of 6 resin volumes and protein was eluted in aliquots of 15 mL with an elution buffer containing 154 mg of reduced L-glutathione in 50 mM Tris-HCl at pH 8. Protein concentration in the samples was measured using a Nanodrop, and purity was assessed on a 4–12% Bis-Tris gel stained using Coomasie Blue. Samples were stored on ice overnight at 4°C. 0.3 mg of Prescission Protease was added to the GST-CTNav1.5-CaM complex per 10 mg of protein. The protein was dialyzed overnight against 50 mM Tris pH 7, 1 mM DTT. The next day, the protein was loaded onto a Source Q column. The eluate from the Source Q column was concentrated to 55 mg mL^{-1} and stored at −80 °C. Purity was assessed at each step by SDS-PAGE electrophoresis. Visual inspection revealed a purity of at least 95%

Crystallization, Data Collection and Structure determination

The CTNa$_v$1.5-CaM wild type and selenomethionine-derivatized protein complex were crystallized by hanging-drop vapor diffusion at 18 °C by 1.2 :0.8 ratio of protein at 35–55 mg mL^{-1} and a well solution containing 15% PEG 4K, 0.2 M $MgSO_4$ and 10% glycerol. Prior to data collection, crystals were transferred to the reservoir solution supplemented with additional glycerol and flash-frozen in liquid nitrogen.

Data for native protein crystals were collected at the home source; MAD data for the selenomethionine-derivatized crystals were collected at APS on the LRL-CAT beamline 31A and at the National Synchrotron Light Source (NSLS) beamline X6A at the Se peak wavelength of 0.97989 Å. Indexing and data reduction were carried out with HKL2000 [38]. The crystal contained five CTNav1.5-CaM complexes in the asymmetric unit (ASU).

Phases were determined with SHARP[39] using data from the SeMet crystal. The positions of 47 out of the 90 seleniums atoms (8 methionine residues in CTNav1.5, 10 methionine residues in CaM with 5 heterodimers in the ASU) were determined by the program followed by phase determination, map calculation, density modification and initial model building to 3.3 Å. Non-crystallographic symmetry (NCS) averaging with the Solomon (density modification) program of the AutoSharp suite [40] was used to extend the phases to 3.0 Å using a solvent content of 55 %. The map generated using these improved phases allowed a combination of automatic and manual tracing of the protein backbone followed by iterative cycles of manual model building with Coot[41] and refinement with Refmac5 in the CCP4i suite [40]

The model of the SeMet-derivatized protein was used as a molecular replacement search model [42]for the native protein, which diffracted to a higher resolution. Model building was completed with iterative cycles of manual model building with Coot and refinement with Refmac5 [40]. The correctness of the alignment of the sequence to the electron density was ascertained using the selenomethionine sites determined in Sharp. The final model was refined to 2.8 Å with R_{work} and R_{free} values of 21.6 and 28.3, respectively (Supplementary Table 1). The quality of the structure was validated with Procheck[43] and Molprobity[44]. 82.6% of residues are in the favored region of the Ramachandran plot, 14.9% in additional allowed region, and no residues in the disallowed region. The final model contains amino

acids 1352 buried surface areas were calculated using Protein Interfaces, Surfaces, and Assemblies (PISA) software[24]. Native data collected at Cu Kα was used to calculate anomalous maps to verify the absence of Ca^{2+} bound to $CTNa_v1.5$-CaM-Mg^{2+}.

Size Exclusion Chromatography

Gel filtration of 200 μL $CTNa_v1.5$-CaM 40 mg mL^{-1} was performed (n=5) on a Superdex 75 10/300 GL column on an AKTA FPLC (GE Lifesciences) in 50 mM Tris Cl pH 7.0, 150 mM NaCl, 1mM DTT with and without 20 mM $MgSO_4$. The protein standards albumin (66 kDa), and carbonic anhydrase (29 kDa) were used to calibrate the column.

Isothermal Calorimetry

ITC experiments were performed with $CTNa_v1.5$ 75 μM and 1mM CaM. The protein in the sample cell was titrated with 25 10 μL injections of CaM. ITC experiments were performed with $CTNa_v1.5$-CaM and III-IV peptide (residues 1489–1502). The protein complex was diluted to a concentration of 40 μM (in monomers) in a buffer containing 10 mM Na_2HPO_4, 2 mM KH_2PO_4, 2.7 mM KCl, 137 mM NaCl, pH 7.4. The III-IV peptide was prepared in the same buffer at a concentration of 0.5 mM. 1.8 mL of protein in the sample cell was titrated with twenty-five 10 μl injections. The data were analyzed with Origin-5.0 software and fitted to a single binding site per monomer.

Cellular Electrophysiology

The $Na_V1.5$ mutations were made by site directed mutagenesis of $Na_V1.5$-GFP cDNAs using the Strategene Quickchange XL kit[14]. Approximately 0.75×10^6 human embryonic kidney cells (HEK293; American Type Culture Collection, Manassas, VA) were cultured in 6-well tissue culture dishes in DMEM supplemented with FBS 10%, L-glutamine (2 mmol L^{-1}). The cells were co-transfected with plasmids encoding the appropriate $Na_V1.5$-GFP and $Na_V\beta1$ subunit cDNAs as previously described [14]. Cells were transfected using Lipofectamine™ 2000 (Invitrogen) according to the manufacturer's instructions and were studied at 48 hrs post-transfection. The total amount of DNA for all transfections was kept constant.

Whole cell I_{Na} was measured under voltage-clamp with an Axopatch 200B patch-clamp amplifier (Molecular Devices Corp.) at room temperature (22°C). Voltage command protocols were generated by custom-written software and PCLAMP 10. Capacitance compensation was optimized and series resistance was compensated by 40–80%. Membrane currents were filtered at 5 kHz and digitized with 12-bit resolution through a DigiData-1200 interface (Molecular Devices Corp.). The patch pipettes had 1–2 MΩ tip resistances when filled with a pipette solution containing: 10 mM NaF, 20 mM CsCl, 100 mM CsF, 10 mM HEPES, 5 mM BAPTA, 4mM CaCl2, pH 7.3 with CsOH. The bath solution contained 145 mM NaCl, 4 mM KCl, 1.8 mM $CaCl_2$, 1 mM $MgCl_2$, 10 mM glucose, 10 mM HEPES (pH 7.4 with NaOH).

Standard voltage clamp protocols were used to characterize the voltage-dependence of activation and inactivation and recovery from inactivation. To determine the $V_{1/2}$ and slope factor k, steady state inactivation data were fit with a Boltzmann function of the form: I/

$I_{max}=\{1+\exp[(V-V_{1/2})/k]\}^{-1}$. Recovery from inactivation data were fit with a bi-exponential function of the form:

$$I(t)/I_{max}=A_1\cdot\exp(-t/\tau_1)+A_2\cdot\exp(-t/\tau_2)+A_3$$

using a nonlinear least squares minimization.

Supplementary Material

Refer to Web version on PubMed Central for supplementary material.

Acknowledgements

This work was funded in part by NIH HL050411. Use of the Advanced Photon Source at Argonne National Laboratory was supported by the U. S. Department of Energy, Office of Science, Office of Basic Energy Sciences, under Contract No. DE-AC02-06CH11357. Use of the Lilly Research Laboratories Collaborative Access Team (LRL-CAT) beam line at Sector 31 of the Advanced Photon Source was provided by Eli Lilly Company, which operates the facility. Data collection was carried out at beam line X6A, funded by the National Institute of General Medical Sciences, National Institute of Health under agreement GM-0080. The NSLS, Brookhaven National Laboratory is supported by the US Department of energy under contract No. DE AC02-98CH10886.

We acknowledge the use and services of the JHU SOM Mass Spectrometry and Proteomics Core, supported by NHI NIDDK center grant P30 DK089502.

The rendition of Fig. 8 was contributed by T. Phelps, M.S.

References

1. Zimmer T, Surber R. SCN5A channelopathies--an update on mutations and mechanisms. Prog Biophys Mol Biol. 2008; 98:120–136. [PubMed: 19027780]
2. Stuhmer W, Methfessel C, Sakmann B, Noda M, Numa S. Patch clamp characterization of sodium channels expressed from rat brain cDNA. Eur Biophys J. 1987; 14:131–138. [PubMed: 2435540]
3. West JW, et al. A cluster of hydrophobic amino acid residues required for fast Na(+)-channel inactivation. Proc Natl Acad Sci U S A. 1992; 89:10910–10914. [PubMed: 1332060]
4. Abriel H. Roles and regulation of the cardiac sodium channel Na v 1.5: recent insights from experimental studies. Cardiovasc Res. 2007; 76:381–389. [PubMed: 17727828]
5. Savio-Galimberti E, Gollob MH, Darbar D. Voltage-gated sodium channels: biophysics, pharmacology, and related channelopathies. Front Pharmacol. 2012; 3:124. [PubMed: 22798951]
6. Cormier JW, Rivolta I, Tateyama M, Yang AS, Kass RS. Secondary structure of the human cardiac Na+ channel C terminus: evidence for a role of helical structures in modulation of channel inactivation. J Biol Chem. 2002; 277:9233–9241. [PubMed: 11741959]
7. Wang C, Chung BC, Yan H, Lee SY, Pitt GS. Crystal structure of the ternary complex of a NaV C-terminal domain, a fibroblast growth factor homologous factor, and calmodulin. Structure. 2012; 20:1167–1176. [PubMed: 22705208]
8. Biswas S, et al. Calmodulin regulation of Nav1.4 current: role of binding to the carboxyl terminus. J Gen Physiol. 2008; 131:197–209. [PubMed: 18270170]
9. Wingo TL, et al. An EF-hand in the sodium channel couples intracellular calcium to cardiac excitability. Nat Struct Mol Biol. 2004; 11:219–225. [PubMed: 14981509]
10. Kim J, et al. Calmodulin mediates Ca2+ sensitivity of sodium channels. J Biol Chem. 2004; 279:45004–45012. [PubMed: 15316014]
11. Sarhan MF, Tung CC, Van Petegem F, Ahern CA. Crystallographic basis for calcium regulation of sodium channels. Proc Natl Acad Sci U S A. 2012; 109:3558–3563. [PubMed: 22331908]
12. Sarhan MF, Van Petegem F, Ahern CA. A double tyrosine motif in the cardiac sodium channel domain III-IV linker couples calcium-dependent calmodulin binding to inactivation gating. J Biol Chem. 2009; 284:33265–33274. [PubMed: 19808664]

13. Deschenes I, et al. Isoform-specific modulation of voltage-gated Na(+) channels by calmodulin. Circ Res. 2002; 90:E49–E57. [PubMed: 11884381]
14. Biswas S, DiSilvestre D, Tian Y, Halperin VL, Tomaselli GF. Calcium-mediated dual-mode regulation of cardiac sodium channel gating. Circ Res. 2009; 104:870–878. [PubMed: 19265034]
15. Haitin Y, Carlson AE, Zagotta WN. The structural mechanism of KCNH-channel regulation by the eag domain. Nature. 2013; 501:444–448. [PubMed: 23975098]
16. Chagot B, Potet F, Balser JR, Chazin WJ. Solution NMR structure of the C-terminal EF-hand domain of human cardiac sodium channel NaV1.5. J Biol Chem. 2009; 284:6436–6445. [PubMed: 19074138]
17. Miloushev VZ, et al. Solution structure of the NaV1.2 C-terminal EF-hand domain. J Biol Chem. 2009; 284:6446–6454. [PubMed: 19129176]
18. Zhang M, Tanaka T, Ikura M. Calcium-induced conformational transition revealed by the solution structure of apo calmodulin. Nat Struct Biol. 1995; 2:758–767. [PubMed: 7552747]
19. Senguen FT, Grabarek Z. X-ray Structures of Magnesium and Manganese Complexes with the N-Terminal Domain of Calmodulin: Insights into the Mechanism and Specificity of Metal Ion Binding to an EF-Hand. Biochemistry. 2012
20. Feldkamp MD, Yu L, Shea MA. Structural and energetic determinants of apo calmodulin binding to the IQ motif of the Na(V)1.2 voltage-dependent sodium channel. Structure. 2011; 19:733–747. [PubMed: 21439835]
21. Meador WE, Means AR, Quiocho FA. Modulation of calmodulin plasticity in molecular recognition on the basis of x-ray structures. Science. 1993; 262:1718–1721. [PubMed: 8259515]
22. Swindells MB, Ikura M. Pre-formation of the semi-open conformation by the apo-calmodulin C-terminal domain and implications binding IQ-motifs. Nat Struct Biol. 1996; 3:501–504. [PubMed: 8646534]
23. Chichili VP, Xiao Y, Seetharaman J, Cummins TR, Sivaraman J. Structural Basis for the Modulation of the Neuronal Voltage-Gated Sodium Channel NaV1.6 by Calmodulin. Sci Rep. 2013; 3:2435. [PubMed: 23942337]
24. Krissinel E, Henrick K. Inference of macromolecular assemblies from crystalline state. J Mol Biol. 2007; 372:774–797. [PubMed: 17681537]
25. Glaaser IW, et al. Perturbation of sodium channel structure by an inherited Long QT Syndrome mutation. Nat Commun. 2012; 3:706. [PubMed: 22426227]
26. Hoshi M, et al. Brugada syndrome disease phenotype explained in apparently benign sodium channel mutations. Circ Cardiovasc Genet. 2014; 7:123–131. [PubMed: 24573164]
27. Clatot J, et al. Dominant-negative effect of SCN5A N-terminal mutations through the interaction of Na(v)1.5 alpha-subunits. Cardiovasc Res. 2012; 96:53–63. [PubMed: 22739120]
28. Krissinel E. Crystal contacts as nature's docking solution. 2009
29. Bell GI. Models for the specific adhesion of cells to cells. Science. 1978; 200:618–627. [PubMed: 347575]
30. Bell GI, Dembo M, Bongrand P. Cell adhesion. Competition between nonspecific repulsion and specific bonding. Biophys J. 1984; 45:1051–1064. [PubMed: 6743742]
31. Wu Y, Vendome J, Shapiro L, Ben-Shaul A, Honig B. Transforming binding affinities from three dimensions to two with application to cadherin clustering. Nature. 2011; 475:510–513. [PubMed: 21796210]
32. Dover K, Solinas S, D'Angelo E, Goldfarb M. Long-term inactivation particle for voltage-gated sodium channels. J Physiol. 2010; 588:3695–3711. [PubMed: 20679355]
33. Liu CJ, Dib-Hajj SD, Renganathan M, Cummins TR, Waxman SG. Modulation of the cardiac sodium channel Nav1.5 by fibroblast growth factor homologous factor 1B. J Biol Chem. 2003; 278:1029–1036. [PubMed: 12401812]
34. Jura N, Shan Y, Cao X, Shaw DE, Kuriyan J. Structural analysis of the catalytically inactive kinase domain of the human EGF receptor 3. Proc Natl Acad Sci U S A. 2009; 106:21608–21613. [PubMed: 20007378]
35. Tan HL, et al. A calcium sensor in the sodium channel modulates cardiac excitability. Nature. 2002; 415:442–447. [PubMed: 11807557]

36. Chagot B, Chazin WJ. Solution NMR structure of Apo-calmodulin in complex with the IQ motif of human cardiac sodium channel NaV1.5. J Mol Biol. 2011; 406:106–119. [PubMed: 21167176]
37. Leahy DJ, Erickson HP, Aukhil I, Joshi P, Hendrickson WA. Crystallization of a fragment of human fibronectin: introduction of methionine by site-directed mutagenesis to allow phasing via selenomethionine. Proteins. 1994; 19:48–54. [PubMed: 8066086]
38. Otwinowski Z, Minor W. Processing of X-ray Diffraction Data Collected in OS. Methods in Enzymology. 1997; Vol. 276:307–326.
39. Bricogne G, Vonrhein C, Flensburg C, Schiltz M, Paciorek W. Generation, representation and flow of phase information in structure determination: recent developments in and around SHARP 2.0. Acta Crystallogr D Biol Crystallogr. 2003; 59:2023–2030. [PubMed: 14573958]
40. Winn MD. Overview of the CCP4 suite and current developments. Acta Crystallogr D Biol Crystallogr. 2011; D67:235–242. [PubMed: 21460441]
41. Emsley P, Lohkamp B, Scott WG, Cowtan K. Features and development of Coot. Acta Crystallogr D Biol Crystallogr. 2010; 66:486–501. [PubMed: 20383002]
42. Navaza J. Implementation of molecular replacement in AMoRe. Acta Crystallogr D Biol Crystallogr. 2001; 57:1367–1372. [PubMed: 11567147]
43. Laskowski R, MacArthur M, Moss D, Thornton JM. PROCHECK- a program to check the stereochemical quality of protein structures. Journal of Applied Crystallography. 1993; 26:283–291.
44. Lovell S, et al. Structure validation by Ca geometry. Proteins: Struct Funct and Genetics. 2003; 50:437–450.

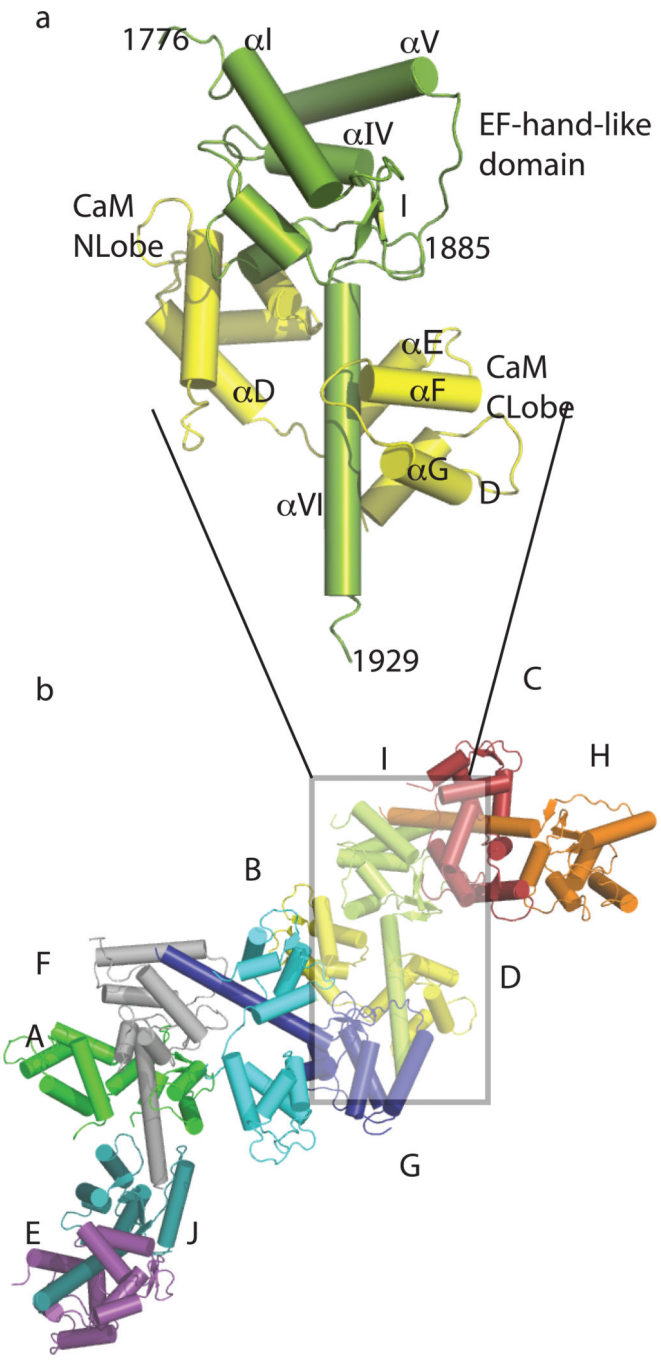

Figure 1. CTNa$_v$1.5-CaM complex

(a) CTNa$_v$1.5-CaM complex with CTNa$_v$1.5 in lime green and CaM in yellow. The helices of CTNa$_v$1.5 are labeled αI-VI and CaM helices αA–G. **(b)**. The five CTNa$_v$1.5-CaM complexes in the asymmetric unit. The CaM molecules are labeled A, B, C, D, and E; the CTNa$_v$1.5 are labeled F, G, H, I, J. For example, AF is the heterodimer with CaM molecule A and CTNa$_v$1.5 molecule F.

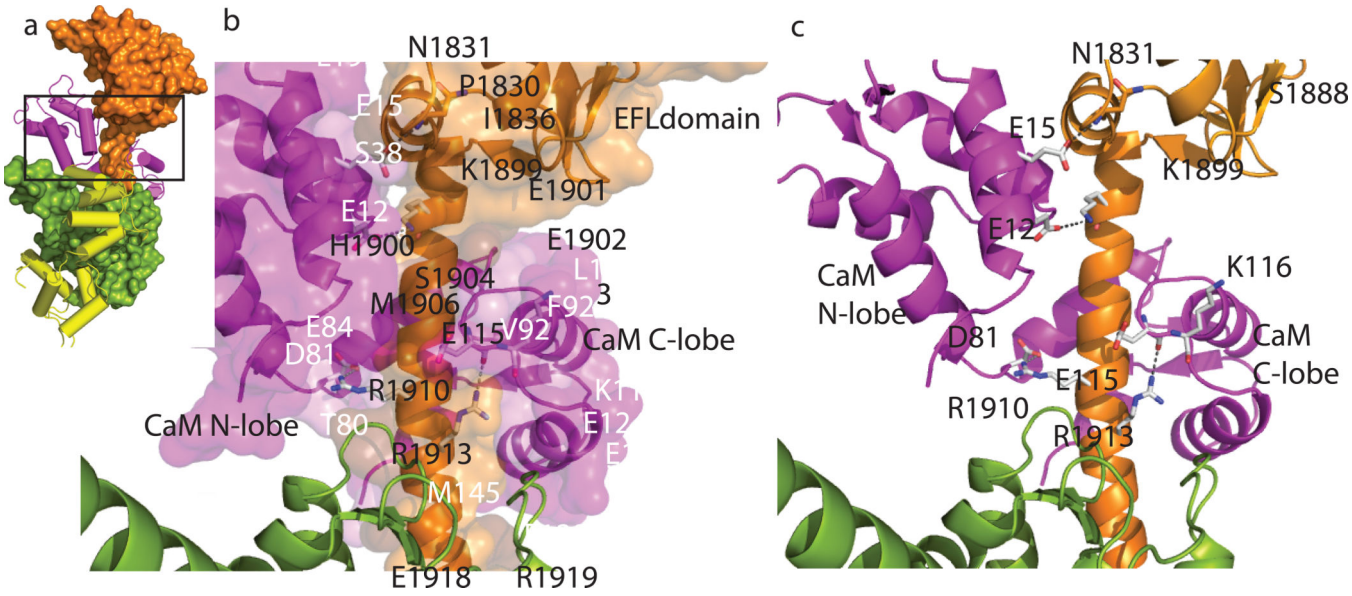

Figure 2. Interaction of CTNa$_v$1.5 with CaM

(a) Overview of the heterodimer. **(b)**. Surface representation of the residues involved at the interface of CT Na$_v$1.5 (orange) and the N- and C- lobe of CaM (magenta). The neighboring CTNa$_v$1.5 is shown in green. **(c)** Hydrogen bonding residues flanking the end of the interface (Glu12-Lys1899; Glu15-Asn1831; Glu115-Arg1913; Asp81-Arg1910)

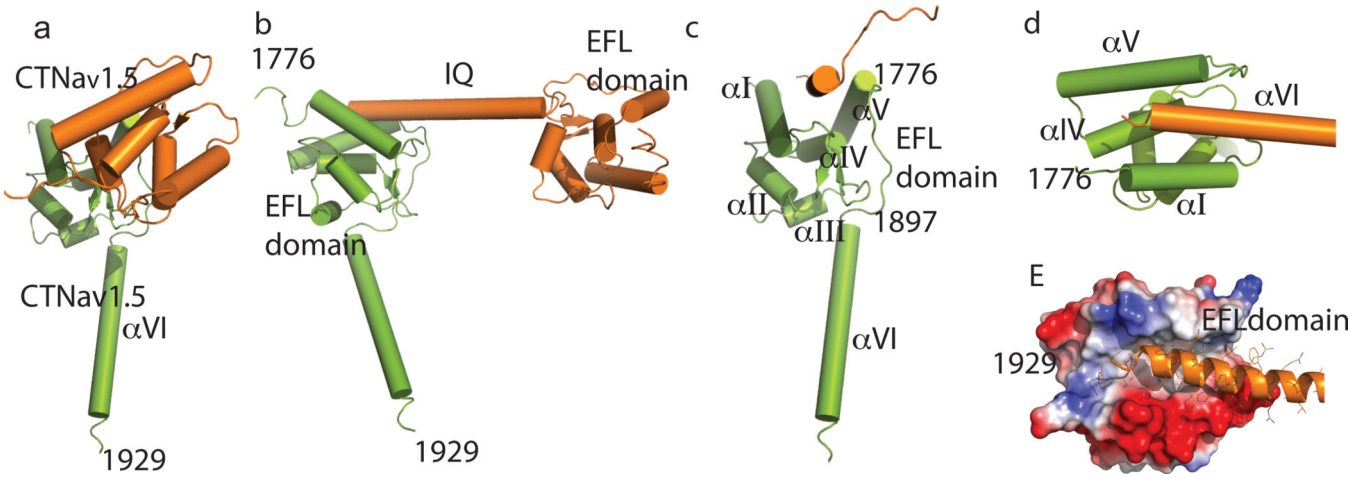

Figure 3. Interaction of the CTNa$_v$1.5 EFL domain with a neighboring CTNa$_v$1.5 helix αVI

(a) Front view of the CTNa$_v$1.5-CTNa$_v$1.5 dimer. Residues of one CTNa$_v$1.5 molecule (green) interact with another CTNa$_v$1.5 molecule (orange). **(b)** Same as panel A but rotated 90 ° from A in the plane of the figure. **(c)**90 ° rotation from panel B showing the concave cavity formed by the helices of EFL domain; helix αI 1788–1801; helix αII 1814–1820; helix αIII 1832–1837; helix αIV 1850–1858; helix αV 1866–1882; helix αVI 1897–1926. **(d)** Close up of the cavity formed by helices αI and αV with helix αVI. **(e)** Same as D but with one CTNa$_v$1.5 colored according to the electrostatic potential. It displays a hydrophobic surface with ionic patches at the beginning and end.

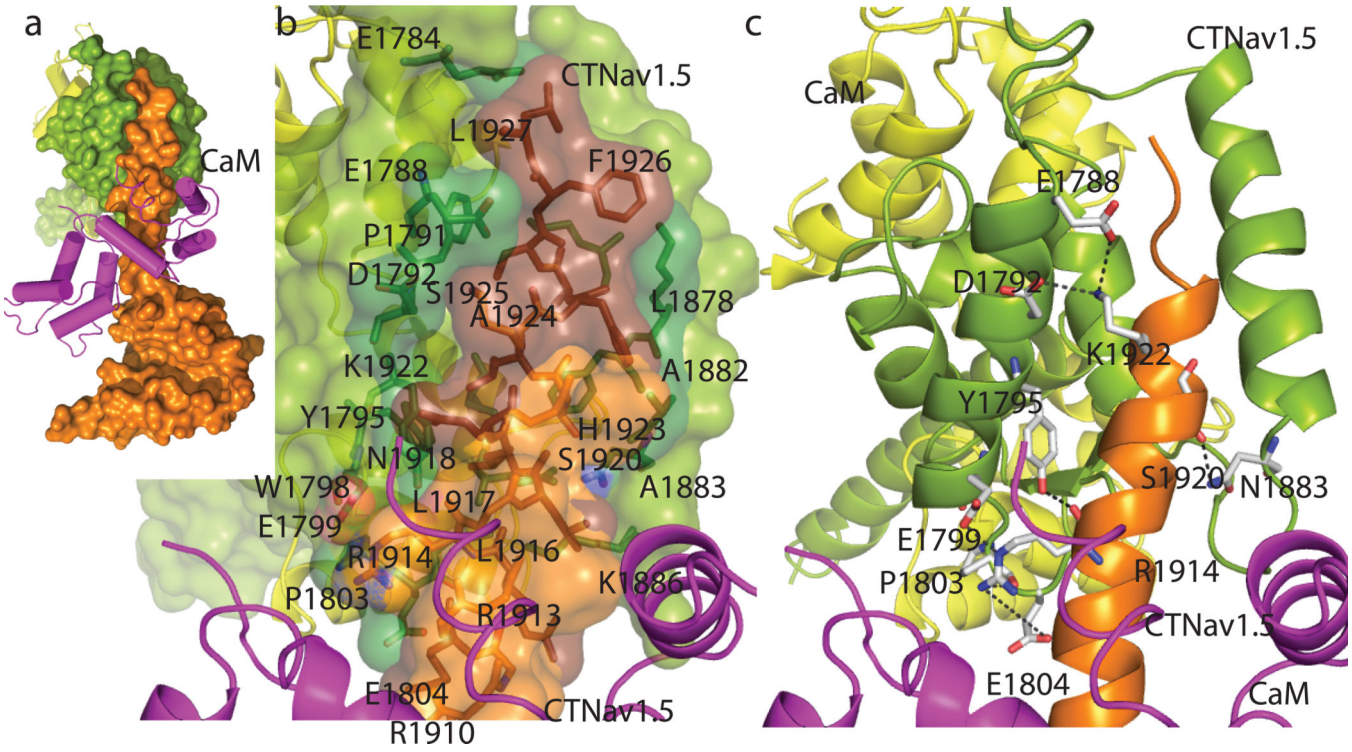

Figure 4. Molecular view of the CTNa$_v$1.5 EFL domain with a neighboring CTNa$_v$1.5 helix αVI

(a) Overview of the Na$_v$1.5-Na$_v$1.5 interaction. (**b**) Surface representation of the residues involved at the interface of CT Na$_v$1.5 helix αVI (orange and brown) with the neighboring CTNa$_v$1.5 EFL (green and forest green) displaying the involved amino acids as sticks. **(c)** Ribbon representation of the interface showing the amino acid at hydrogen bonding distance. Hydrogen bonding pattern of CTNa$_v$1.5 EFL (green and forest green) with the CTNa$_v$1.5 (orange and brown).

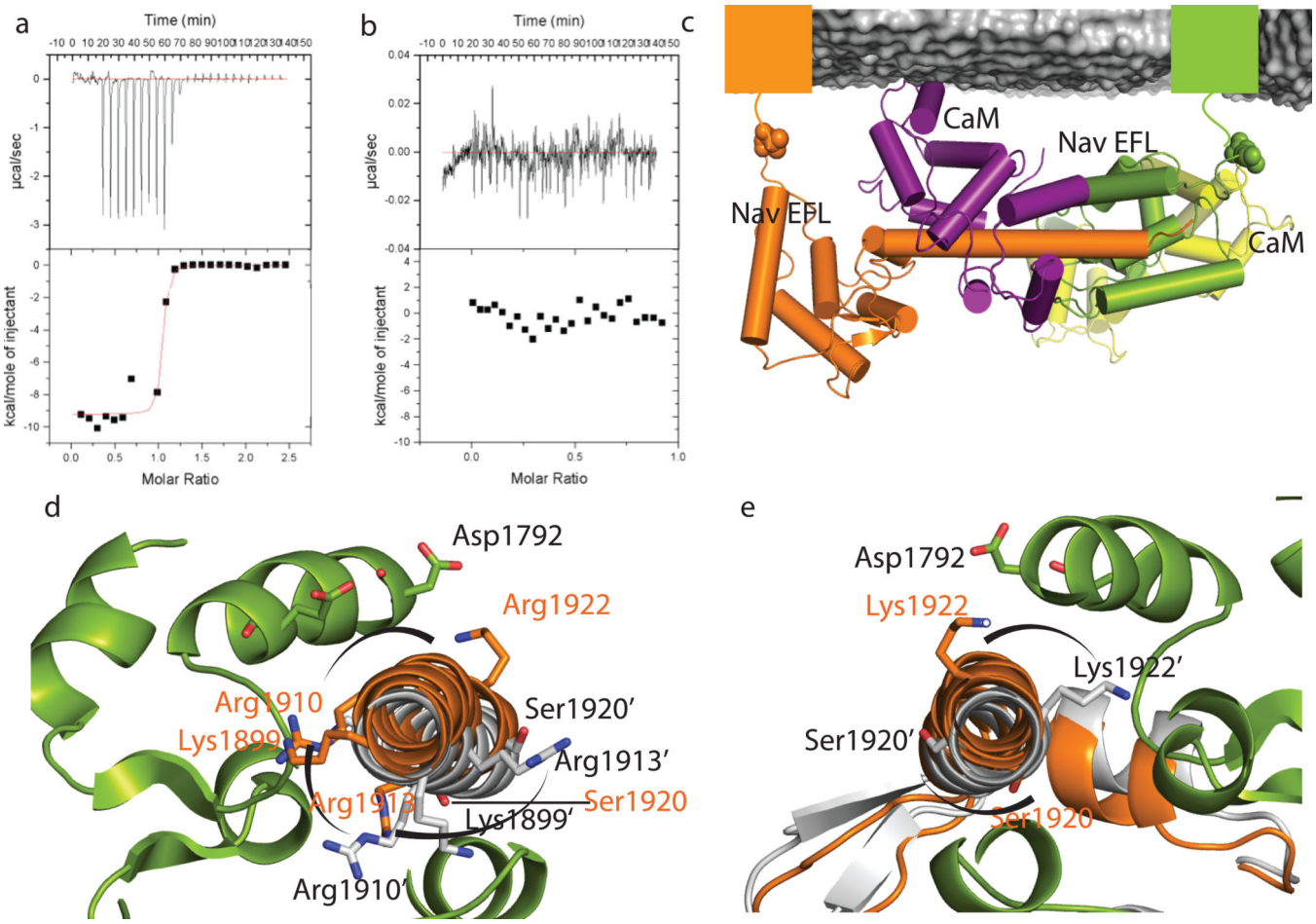

Figure 5. Non-inactivated conformation of CTNa$_v$1.5-CaM

(**a**) Thermodynamic analysis of CTNa$_v$1.5 and CaM binding. Isotherms of CTNa$_v$1.5 titrated with CaM. Top panel display the heat evolved following each injection and the bottom panel shows the integrated heats of injection. All the curves are fitted to a one-binding site per monomer model.(b). Thermodynamic analysis of CTNa$_v$1.5-CaM and III-IV linker binding. Isotherm of CTNav1.5-CaM titrated with the III-IV linker (residues 1489–1502). (panels as in a). Note the change in scale on the *y* axis. **(c)**. Attachment points of the N-termini of the CTNa$_v$1.5 (colored squares) to the trans-membrane helices S6 of domain IV of the channel (not shown). **(d)**. Overlap of CT helices αVI in the resting non- inactive conformation (orange) versus inactivated (grey). The rotation of the helix αVI is evidenced by the rotated positions of Lys1899, Arg1910, Arg1913, and Ser1920. This change highlights the disruption of the CTNa$_v$1.5-CTNa$_v$1.5 interaction caused by the rotation that results in the inactivated form of the channel. **(e)**. Same as (d) but seen from the C-terminal of helix αVI of the CTNa$_v$1.5.

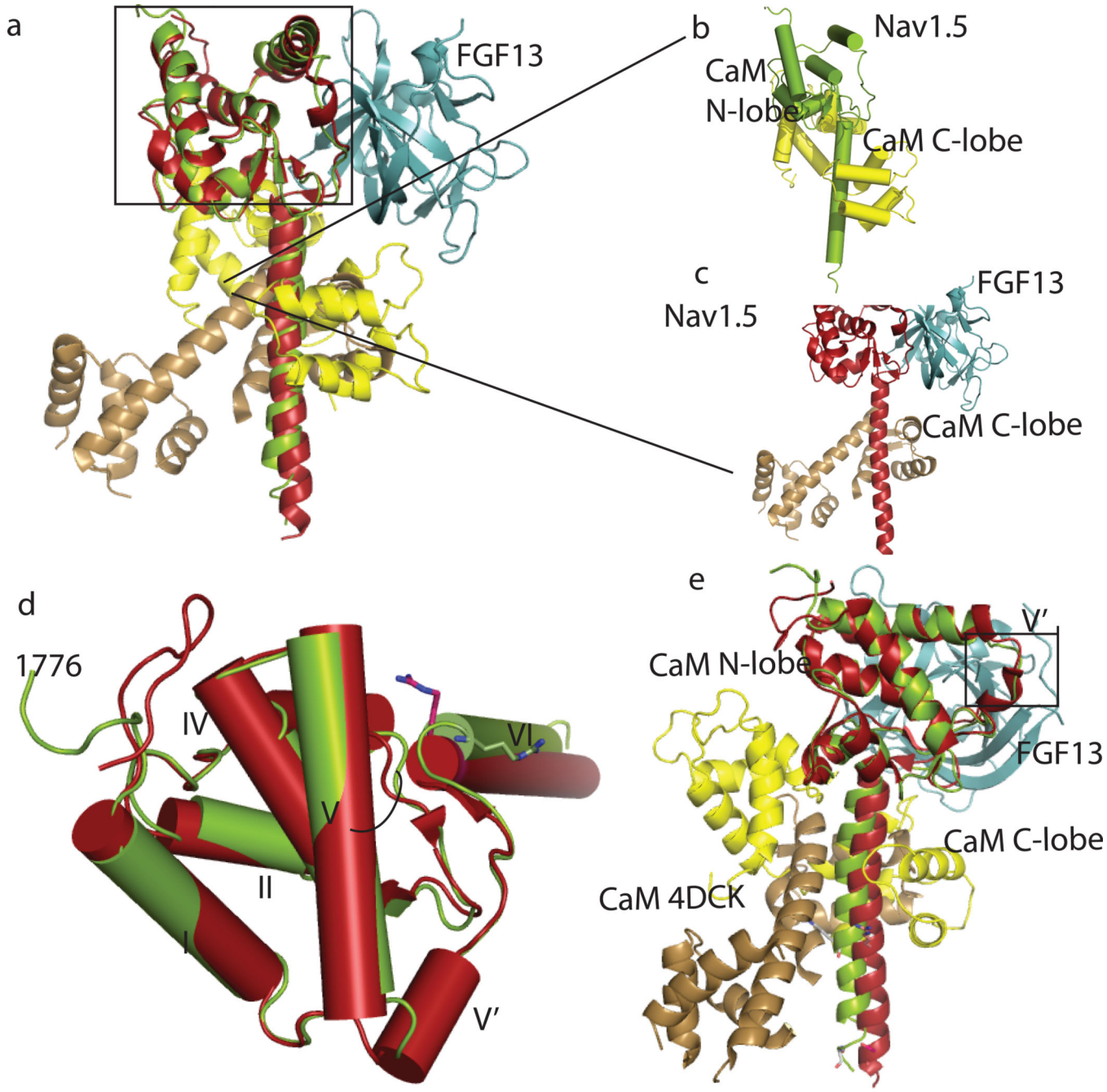

Figure 6. Overlap of CTNa$_v$1.5-CaM with Na$_v$1.5-CaM-FGF13 aligning their EFL domains

(**a**) CTNa$_v$1.5-CaM is shown in lime-green/yellow (this work; PDB 4OVN). **(b)** The alignment highlights the rotation of helix αVI by 90° with respect to the EFL domain. The CaM rotates with the helix. CTNav1.5-CaM is shown in lime-green/yellow (this work) and Na$_v$1.5-CaM-FGF13 (PDB 4DCK, red; CaM, sand, FHF in cyan). **(c)** Nav1.5-CaM-FGF13 (PDB 4DCK). **(d)** Close-up of the EFL area boxed in panel a; Na$_v$1.5-CaM-FGF13 has an extra helix V'. **(e)** Overlap of CTNa$_v$1.5-CaM with Na$_v$1.5-CaM-FGF13 showing that the extended conformation of CaM is not conducive to the formation of a CTNa$_v$1.5-CTNa$_v$1.5

dimer; two residues in helix VI show the rotation of the helix. The residues shown are part of the charge-charge interaction of $Na_v1.5$ IQ-CaM.

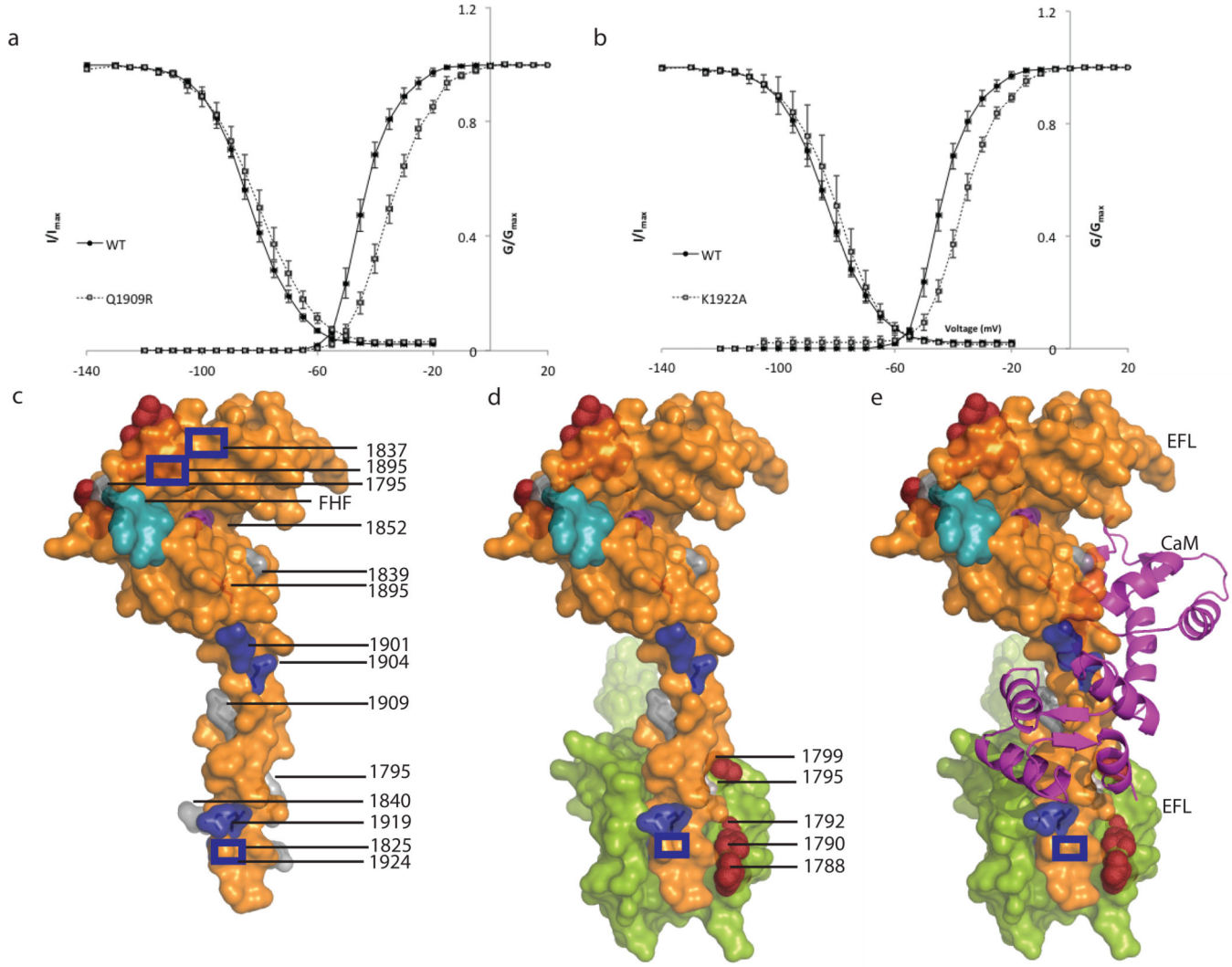

Figure 7. Mutations affecting CTNa$_v$1.5-CaM and CTNa$_v$1.5-CTNa$_v$1.5 interactions

(a) and (b). Electrophysiological features of Na^+ channel variants altered at the *CTNa$_v$1.5-CaM*-Ca^{2+} interaction interface. Activation and steady state inactivation of wild type (circles) and mutant channels (squares). The data are fit to a Boltzman function as described in Methods. Mutant channels and Q1909R and K1922A exhibit a depolarizing shift in the $V_{0.5}$ of inactivation (Supplementary Fig. 5). **(c)** Surface representation of one monomer (orange) interacting with a neighboring molecule (lime green). CTNa$_v$1.5 with LQT3 mutations (1795,1825, 1840,1895,1909 and 1924) shown in grey and brugada syndrome mutations in blue (1837,1901,1904,1919). Epilepsy mutations at the interface with CaM-C-term lobe (1895 and 1852) are shown in purple; Brugada mutations (1901 and 1904) are at the interface of CTNa$_v$1.5 with the CaM-C-term lobe (blue) and 1705, 1825, 1840, 1924 are at the CTNa$_v$1.5-CTNa$_v$1.5 interface. Residues 1788, 1790, 1792, 1799, shown in dark red, line the EFL binding site for helix αVI residues past the IQ motif [14]. Residues of the FGF13 that contact the EFL domain are colored turquoise. **(d)** Same as (c) displaying the neighboring *CTNa$_v$1.5***(e)** Same orientation as in panels c and d including CaM as a magenta ribbon.

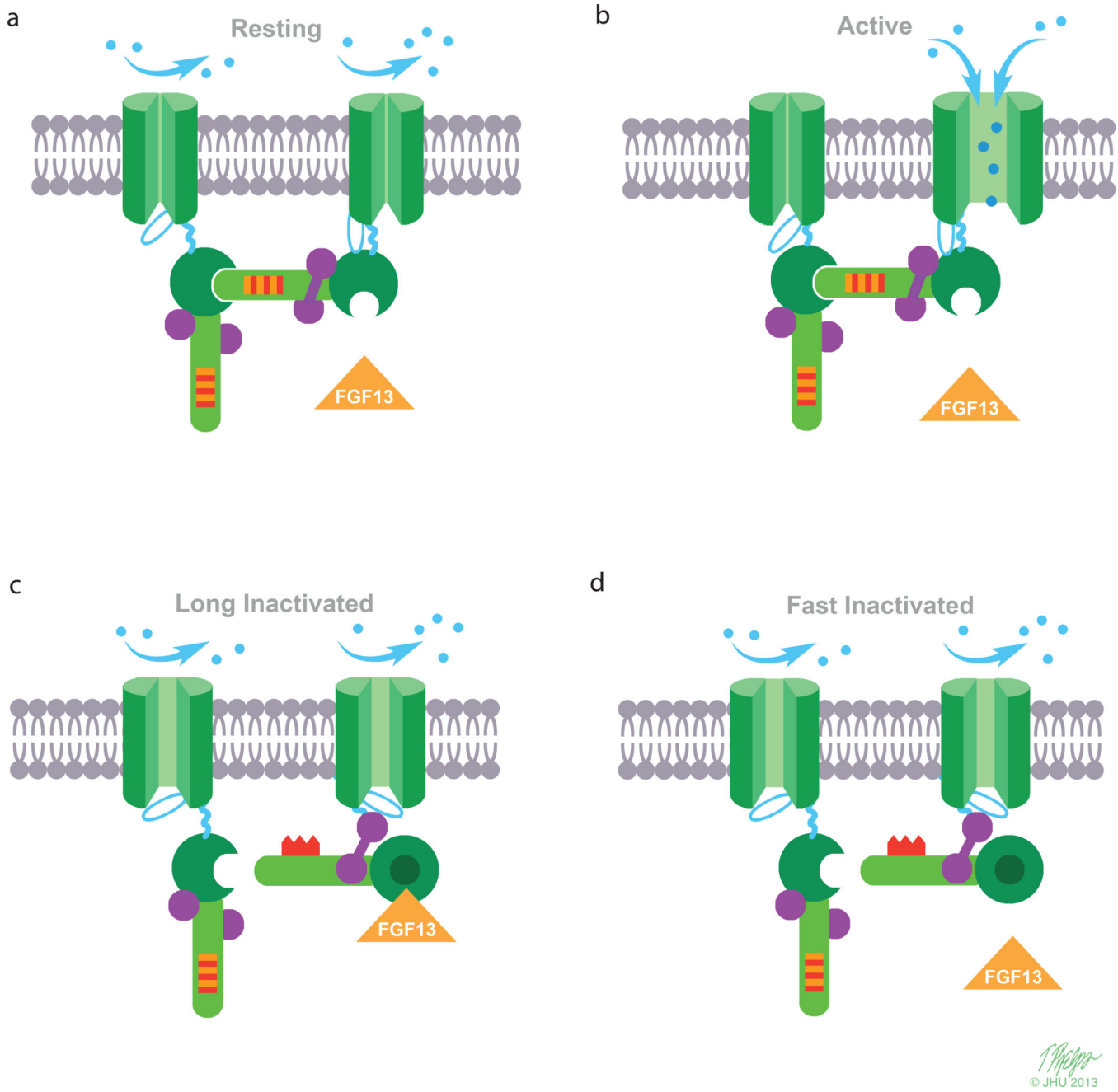

Figure 8. Proposed mechanism of $Na_v1.5$ regulation by the $Na_v1.5$ cytoplasmic domain

$Na_v1.5$ is colored in green with a serrated marker in helix αVI to highlight the 90° rotation. Calmodulin is shown in purple. **(a)** Resting state showing the *intermolecular* interaction of the $Na_v1.5$ poised for activation. **(b)** Active. N-lobe of CaM interacts with the EFHL domain of Nav1.5; C-lobe of CaM interacts with IQ of helix αVI. **(c)** Long inactivated. FGF13 bound to the EFHL. **(d)** Fast inactivated. N-lobe of CaM releases the EFH-like and possible interacts with III-IV linker. Helix αVI rotates 90 degrees

Table 1

Data collection and refinement statistics

	Crystal 1 $CTNa_v1.5$-CaM-Mg^{2+}		**Crystal 2 CTNav1.5-CaM-Mg^{2+}**
Data collection			
Space group	$P2_1$		$P2_1$
Cell dimensions			
a, *b*, *c* (Å)	106.0, 98.4,109.2		106.1, 99.0, 109.2
α, β, γ (°)	90.0, 106.4, 90.0		90.0, 106.1, 90.0
Wavelength (Å)	0.9793 (IP)	0.9537 (RM)	0.97929
Resolution (Å)	50.0–3.2 (3.26–3.20)	50.0–3.2 (3.26–3.20)	50.0–2.8 (2.85–2.80)
R_{sym}	0.12(0.87)	0.13(0.89)	0.11 (0.74)
$I / \sigma I$	15.57 (2.30)	15.0 (2.10)	32.8(1.90)
Completeness (%)	99.9 (99.9)	99.9 (99.9)	90.3 (58.3)
Redundancy	4.6(4.5)	3.2(3.2)	3.3 (2.3)
Refinement			
Resolution (Å)			50.0–2.8
No. reflections			311,500
R_{work} / R_{free}			21.6/28.6
No. atoms			
Protein			11,710
Ligand/ion			66
Water			89
B factors			
Protein			81.2
Ligand/ion			
Water			95.0
r.m.s. deviations			
Bond lengths (Å)			0.011
Bond angles (°)			1.8

Table 2

Effect of CTNa$_v$1.5 mutations on steady state activation and inactivation.

	Activation		**Inactivation**		**Recovery from inactivation**
	$V_{0.5}$ (mV)	K	$V_{0.5}$ (mV)	K	t_{fast} (sec)
WT[a]	−42.8±1.2 (12)	5.49±0.4	−83.0±1 (19)	3.35±0.1	5.5±0.5 (10)
Q1909R[a]	−34.3±1.4 (9)*	3.81±0.2*	−80.6±2.7 (8)	2.96±0.1*	5.1±0.7 (7)
R1910A[a]	−43.2±2.2 (7)	5.63±0.6	−86.0±2.1 (6)	3.60±0.1	6.0±0.5 (6)
R1910E[a]	−41.4±4.5(3)	5.53±1.5	−79.7±2 (3)	3.22±0.3	4.80±0.8(3)
K1922A[a]	−36.2±1.3(4)*	4.09±0.3	−80.9±3.1 (4)	3.42±0.3	5.20±0.8(4)
K1922E[a]	−44.9±2.0 (6)	5.46±0.3	−78.4±1.7(3)	3.55±0.3	6.21±1.7(4)
R1914A[a]	−39.8±1.9(8)	4.33±0.3*	−82.2±3(6)	3.14±0.2	5.8±0.5(5)
R1914E[a]	−39.0±2.5 (5)	4.50±0.6	−79.4±3.7(4)	2.97±0.1*	5.38±1.5(4)
WT[a]	−36 ± 2 (7)		−82.6±0.1 (5)		3.8±0.4 (5)
WT[b]	−38 ± 2 (10)		−87.5±0.2 (14)		5.5±0.1 (9)
D1790G[a,c]	−38.9±0.5 (6)		−96.5±0.1 (6)		3.5±0.3 (5)
4XD1790G[a,c]	−37.4±1.7 (6)		−99.9±0.1 (6)		14.9±0.2 (7)
4X-IQ/AA[a,c]	−32.3 ± 2 (18)		−100.8 ± 0.3 (9)		18.2±0.5 (6)
D1885[b]	−34.1 ± 0.8 (18)		−93.3 ± 0.1 (18)		5.3±0.1 (9)
IQ/AA[b]	−32.7±2.6 (8)		−82.5±0.4 (8)		7.8±1.3 (7)

Values are means SE (n).

[a] in the presence of 0.5 mM/L Ca^{2+};

[b] are with nominally Ca^{2+}-free.

[c] 4X represents the mutations E1788A/D1790A/D1792A/E1799A published in Biswas et al.

* denotes $p<0.05$ compared to WT.